J|A|C|S
ARTICLES
Published on Web 04/01/2006

Ordered Mesoporous Fe_2O_3 with Crystalline Walls

Feng Jiao,[†] Andrew Harrison,[#] Jean-Claude Jumas,[‡] Alan V. Chadwick,[§] Winfried Kockelmann,[¶] and Peter G. Bruce*,[†]

Contribution from the School of Chemistry and EaStChem, University of St. Andrews, St. Andrews, Fife KY16 9ST, U.K., School of Chemistry and EaStChem, University of Edinburgh, Joseph Black Building, West Mains Road, Edinburgh EH9 3JJ, U.K., Laboratoire des Agrégats Moléculaires et Matériaux Inorganiques, UMR 5072, Université Montpellier II, CC 15, Place Eugène Bataillon, 34095, Montpellier Cedex 5, France, ISIS Facility, Rutherford Appleton Laboratory, Chilton OX11 0QX, and Centre for Materials Research, School of Physical Sciences, University of Kent, Canterbury, Kent CT2 7NR, U.K.

Received December 14, 2005; E-mail: pgb1@st-andrews.ac.uk

Abstract: α-Fe_2O_3 has been synthesized with an ordered mesoporous structure and crystalline walls that exhibit a near-single crystal-like order. The unique magnetic behavior of the material, distinct from bulk nanoparticles of α-Fe_2O_3 or mesoporous Fe_2O_3 with disordered walls, has been established. Magnetic susceptibility, Mössbauer, and neutron diffraction data show that the material possesses the same long-range magnetic order as bulk α-Fe_2O_3, despite the wall thickness being less than the 8 nm limit below which magnetic ordering breaks down in nanoparticulate α-Fe_2O_3, yet the Morin transition of bulk α-Fe_2O_3 is absent. It is also shown by TEM, PXRD, and EXAFS that α-Fe_2O_3 with the same ordered mesoporous structure but disordered walls contains small crystalline domains. Mössbauer and magnetic susceptibility data demonstrate that this material exhibits no long-range magnetic order but superparamagnetic behavior.

Introduction

The preparation of open shell transition metal oxides in the form of mesoporous solids (pore sizes 20−150 Å) endows such materials with unique properties.[1−3] The porosity permits access to a large internal transition metal oxide surface where catalytic processes can occur and the confined dimensions of the transition metal oxide walls, between the pores, can change significantly the electrical, magnetic, and optical properties of the materials.

The formation of mesoporous silicas, alumino-silicates, alumino-phosphates, and related materials is already well established.[4−7] It has, however, proved significantly more difficult to synthesize transition metal oxides in the form of mesoporous materials. Pioneering work achieved success with compounds, such as Nb_2O_5, TiO_2, ZrO_2, WO_3, and MnO_x, using soft templating (surfactant) methods, including ligand-assisted templating.[1,8−11] Recently, hard templating methods have been introduced.[12−17] Typically, such methods employ a mesoporous silica as the hard template into which a solution-based precursor of the desired phase is introduced, and following heating to form the desired phase, the silica template is dissolved away to leave a replica mesoporous structure of the target compound. The hard templating route has opened the way to more mesoporous transition metal oxides. However, this method also has its limitations; the resulting materials must be stable in HF or NaOH solution, and the precursors must not react with the silica template at high temperature. For example, in the formation of lithium transition metal oxides, it is necessary to first form the transition metal oxide as a mesoporous solid to avoid Li reaction with the silica template, then to react the mesoporous transition metal solid with a lithium source, such as LiOH.[18]

Iron oxides represent a particularly important class of materials capable of use in a wide range of applications, including catalysis, in magnetic devices, and in rechargeable lithium batteries. They combine such functionality with low cost and low toxicity.[19−21] Porous Fe_2O_3 with disordered and ordered

[†] University of St. Andrews.
[#] University of Edinburgh.
[‡] University of Montpellier.
[¶] Rutherford Appleton Laboratory.
[§] University of Kent.

(1) Behrens, P. *Angew. Chem., Int. Ed. Engl.* **1996**, *35*, 515.
(2) Schüth, F. *Chem. Mater.* **2001**, *13*, 3184.
(3) He, X.; Antonelli, D. *Angew. Chem., Int. Ed.* **2002**, *41*, 214.
(4) Corma, A. *Chem. Rev.* **1997**, *97*, 2373.
(5) Stein, A.; Melde, B. J.; Schroden, R. C. *Adv. Mater.* **2000**, *12*, 1403.
(6) Soler-illia, G. J. D.; Sanchez, C.; Lebeau, B.; Patarin, J. *Chem. Rev.* **2002**, *102*, 4093.
(7) Cundy, C. S.; Cox, P. A. *Chem. Rev.* **2003**, *103*, 663.
(8) Antonelli, D. M.; Ying, J. Y. *Angew. Chem., Int. Ed. Engl.* **1995**, *34*, 2014.
(9) Antonelli, D. M.; Nakahira, A.; Ying, J. Y. *Inorg. Chem.* **1996**, *35*, 3126.
(10) Tian, Z.; Tong, W.; Wang, J.; Duan, N.; Krishnan, V. V.; Suib, S. L. *Science* **1997**, *276*, 926.
(11) Yang, P.; Zhao, D.; Margolese, D. I.; Chmelka, B. F.; Stucky, G. D. *Nature* **1998**, *396*, 152.
(12) Ryoo, R.; Joo, S. H.; Kruk, M.; Jaroniec, M. *Adv. Mater.* **2001**, *13*, 677.
(13) Li, Z. J.; Jaroniec, M. *J. Am. Chem. Soc.* **2001**, *123*, 9208.
(14) Lee, J. S.; Joo, S. H.; Ryoo, R. *J. Am. Chem. Soc.* **2002**, *124*, 1156.
(15) Wang, Y. Q.; Yang, C. M.; Schmidt, W.; Spliethoff, B.; Bill, E.; Schuth, F. *Adv. Mater.* **2005**, *17*, 53.
(16) Zhu, K. K.; Yue, B.; Zhou, W. Z.; He, H. Y. *Chem. Commun.* **2003**, *1*, 98.
(17) Tian, B. Z.; et al. *J. Am. Chem. Soc.* **2004**, *126*, 865.
(18) Jiao, F.; Shaju, K. M.; Bruce, P. G. *Angew. Chem., Int. Ed.* **2005**, *44*, 6550.
(19) Jiao, F.; Yue, B.; Zhu, K. K.; Zhao, D. Y.; He, H. Y. *Chem. Lett.* **2003**, *32*, 770.

10.1021/ja0584774 CCC: $33.50

mesoporous structures have been prepared using soft templating methods.[22−26] However, such methods invariably lead to mesoporous materials with amorphous walls. Hard templating offers an alternative route to the formation of mesoporous Fe_2O_3. Fabrication of Fe_2O_3 by such a route has been reported as part of a wider study of mesoporous transition metal oxides, but few details were given.[17] Although, in general, the formation of mesoporous transition metal oxides by hard templating yields materials with highly crystalline walls, this has not been the case for Fe_2O_3.[15−18] Yet such crystallinity is expected to have an important influence on the properties of the resulting mesoporous materials, especially their magnetic behavior. It is therefore critical to synthesize ordered mesoporous Fe_2O_3 with crystalline walls. Here we demonstrate, for the first time, the synthesis of ordered mesoporous Fe_2O_3 with highly crystalline walls. We also show that the magnetic properties of the material are unique, differing from bulk α-Fe_2O_3, nanoparticulate α-Fe_2O_3, and mesoporous Fe_2O_3 with disordered walls.

Experimental Section

In a typical synthesis of mesoporous α-Fe_2O_3, 1 g of $Fe(NO_3)_3 \cdot 9H_2O$ (98% Aldrich) was dissolved in 20 mL of ethanol followed by addition of 1 g of mesoporous silica, KIT-6. The silica template was prepared according to the procedure described by Ryoo and coworkers.[27] After stirring the mixture at room temperature until nearly dry powder had been obtained, the sample was heated slowly to 300 °C and calcined at that temperature for 3 h. The impregnation procedure was repeated, followed by calcination at 500 °C for 3 h, resulting in mesoporous α-Fe_2O_3 with disordered walls. For the synthesis of mesoporous α-Fe_2O_3 with ordered walls, 1.5 g of $Fe(NO_3)_3 \cdot 9H_2O$ (98% Aldrich) was used. After being stirred at room temperature until a fine and completely dry powder was formed, the sample was heated slowly to 600 °C and kept at that temperature for 6 h. Such differences in the synthesis conditions are sufficient to change significantly the atomic ordering within the walls and have a profound influence on the magnetic behavior, as demonstrated later. The resulting samples were treated three times with hot 2 M NaOH to remove the silica template, centrifuged, washed several times with water and ethanol, then dried at 60 °C in air.

Transmission electron microscopy (TEM) was carried out using a JEOL JEM-2011. Wide-angle powder X-ray diffraction data were collected on a Stoe STADI/P powder diffractometer operating in transmission mode and with a small angle position sensitive detector. Incident radiation was generated using an $Fe_{K\alpha 1}$ source ($\lambda = 1.936$ Å). Small-angle powder X-ray diffraction was carried out using a Rigaku/MSC, D/max-rB with $Cu_{K\alpha 1}$ radiation ($\lambda = 1.541$ Å) and a scintillation detector. Nitrogen adsorption−desorption measurements were conducted using a Hiden IGA porosimeter. ^{57}Fe Mössbauer spectra were recorded in transmission geometry on a standard EG&G spectrometer in the constant acceleration mode, using ^{57}Co(Rh). The hyperfine parameters δ (isomer shift) and Δ (quadrupole splitting) were determined by fitting Lorentzian lines to the experimental data, making use of the ISO program.[28] All isomer shifts are given with respect to the room temperature spectrum of α-Fe. Oxidation states were verified by XANES, and local structure was probed by EXAFS on Station 9.3 at the CCLRC Daresbury Laboratory SRS, U.K. Magnetization data were taken for both materials on a Quantum Design SQUID magnetometer from 1.8 to 300 K, in fields of 0.01 T after cooling first in zero field, and then in 0.01 T field. Data were also taken on a sample of bulk α-Fe_2O_3, synthesized in the same manner as the mesoporous samples but without the silica template.

To explore the cooperative magnetism in mesoporous α-Fe_2O_3 with ordered walls in greater detail, neutron powder diffraction patterns were taken of this form of the material at approximately 298 K on the diffractometer ROTAX at the ISIS Facility, Rutherford Appleton Laboratory, U.K. The lattice parameters and the diffraction peak profile parameters were determined using a LeBail fit as implemented in the GSAS suite of programs.[29] The shapes of the broadened peaks were modeled using pure Lorentzian functions. Crystal and magnetic structural parameters were refined using the Rietveld code in GSAS. An empirical absorption parameter for the wavelength-specific absorption of neutrons by the sample was refined.

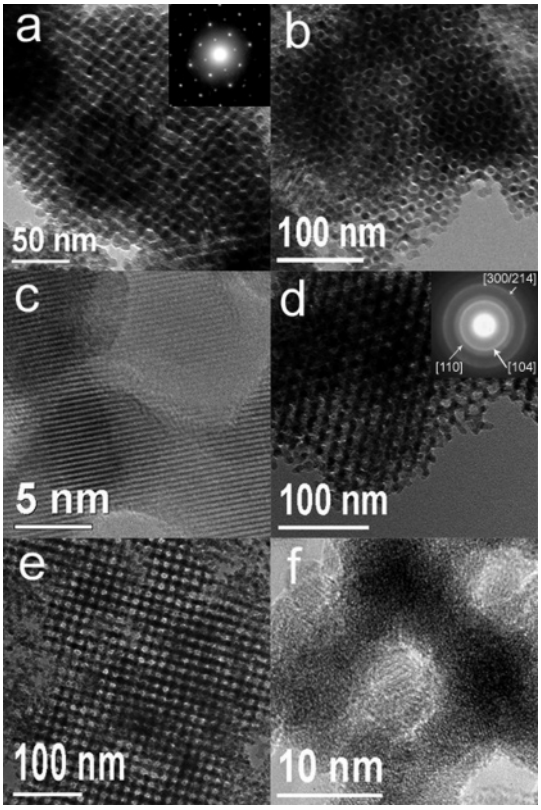

Figure 1. TEM images for mesoporous α-Fe_2O_3 with ordered walls recorded along (a) [110] and (b) [111] directions; HRTEM image of (b) is shown in (c); TEM images for mesoporous α-Fe_2O_3 with disordered walls recorded along (d) [111] and (e) [100] directions; HRTEM image of (e) is shown in (f). SAED patterns for mesoporous α-Fe_2O_3 with ordered walls (a, inset) and with disordered walls (d, inset).

Results and Discussion

Mesoporous Structure. Transmission electron micrographs (TEM) of mesoporous Fe_2O_3 with ordered and disordered walls are shown in Figure 1. The first three images, a−c, show increasingly magnified regions of α-Fe_2O_3 with ordered mesoporous and crystalline walls. Figure 1d−f shows the corresponding views of the α-Fe_2O_3 with ordered mesopores but disordered walls. In both cases, the mesoporous structure is

(20) Ziolo, R. F.; Giannelis, E. P.; Weinstein, B. A.; Ohoro, M. P.; Ganguly, B. N.; Mehrotra, V.; Russell, M. W.; Huffman, D. R. *Science* **1992**, *257*, 219.
(21) Larcher, D.; Masquelier, C.; Bonnin, D.; Chabre, Y.; Masson, V.; Leriche, J. B.; Tarascon, J. M. *J. Electrochem. Soc.* **2003**, *150*, A133.
(22) Srivastava, D. N.; Perkas, N.; Gedanken, A.; Felner, I. *J. Phys. Chem. B* **2002**, *106*, 1878.
(23) Malik, A. S.; Duncan, M. J.; Bruce, P. G. *J. Mater. Chem.* **2003**, *13*, 2123.
(24) Long, J. W.; Logan, M. S.; Rhodes, C. P.; Carpenter, E. E.; Stroud, R. M.; Rolison, D. R. *J. Am. Chem. Soc.* **2004**, *126*, 16879.
(25) Jiao, F.; Bruce, P. G. *Angew. Chem., Int. Ed.* **2004**, *43*, 5958.
(26) Lezau, A.; Trudeau, M.; Tsoi, G. M.; Wenger, L. E.; Antonelli, D. *J. Phys. Chem. B* **2004**, *108*, 5211.
(27) Kleitz, F.; Choi, S. H.; Ryoo, R. *Chem. Commun.* **2003**, 2136.
(28) Kündig, W. *Nucl. Instrum. Methods* **1969**, *75*, 336.
(29) Larson, A. C.; Von Dreele, R. B. *General Structure Analysis System (GSAS)*; Los Alamos National Laboratory Report LAUR 86-748, 1994.

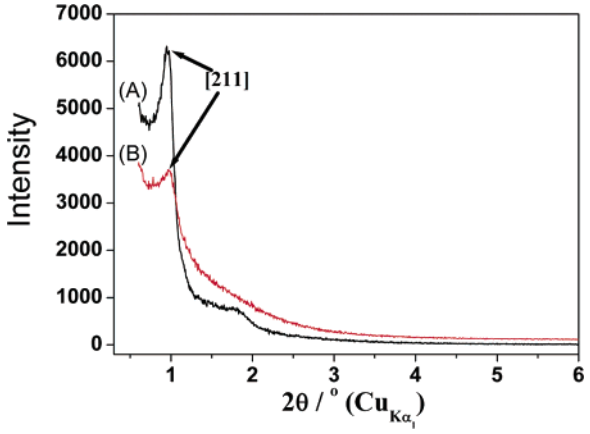

Figure 2. Low-angle XRD patterns for mesoporous α-Fe_2O_3 (A) with ordered walls and (B) with disordered walls.

highly regular, with a $Ia\bar{3}d$ symmetry, replicating that of the KIT-6 silica template used in their formation.[30] On the basis of the TEM data, at least 90% of the α-Fe_2O_3 particles with ordered or disordered walls exhibit an ordered mesoporous structure. In the case of α-Fe_2O_3 with crystalline walls, the lattice repeat, a_0, is 232 Å, whereas for the mesopore with disordered walls, $a_0 = 210$ Å.

Low-angle powder X-ray diffraction data for the two forms of mesoporous α-Fe_2O_3 are shown in Figure 2. Considering first the low-angle data for the highly crystalline material, two peaks are evident with the lower peak, a [211] reflection in space group $Ia\bar{3}d$, corresponding to an a_0 parameter of 229 Å, in good agreement with the a_0 parameter, 232 Å, obtained from TEM images (Figure 1). Although the degree of mesoporous ordering appeared from the TEM data to be similar for α-Fe_2O_3 with and without ordered walls, only a single peak is evident in the low-angle diffraction data of the latter. The low-angle PXRD peak in Figure 2B corresponds to a unit cell parameter of 221 Å, in good agreement with the data calculated from TEM analysis (210 Å). This is ∼4% smaller than that for the crystalline material, indicating that the differences in the degree of ordering within the walls have an effect on the mesoporous structure.

To examine the pore size and its distribution, nitrogen adsorption−desorption measurements were carried out (Figure 3). In both cases, a type IV isotherm is observed. For the material with disordered walls, the type IV isotherm is less well defined, which may be caused by a contribution from interparticle voids. However, the isotherms are similar to those observed for other mesoporous transition metal oxides formed by hard templating.[15] The pore size distributions, calculated from the desorption isotherms, are shown in the inset in Figure 3. For mesoporous α-Fe_2O_3 with ordered walls, the pore size is centered at a diameter of 3.85 nm, and this is in good agreement with the pore diameters anticipated for a replica structure of KIT-6; see, for example, mesoporous Co_3O_4.[18] For the sample with disordered walls, the pore size distribution is slightly wider and centered at a diameter of 3.78 nm, which is slightly smaller than the ordered material. The surface areas estimated from the Brunauer−Emmett−Teller (BET) method were also obtained from the nitrogen adsorption−desorption measurements and are

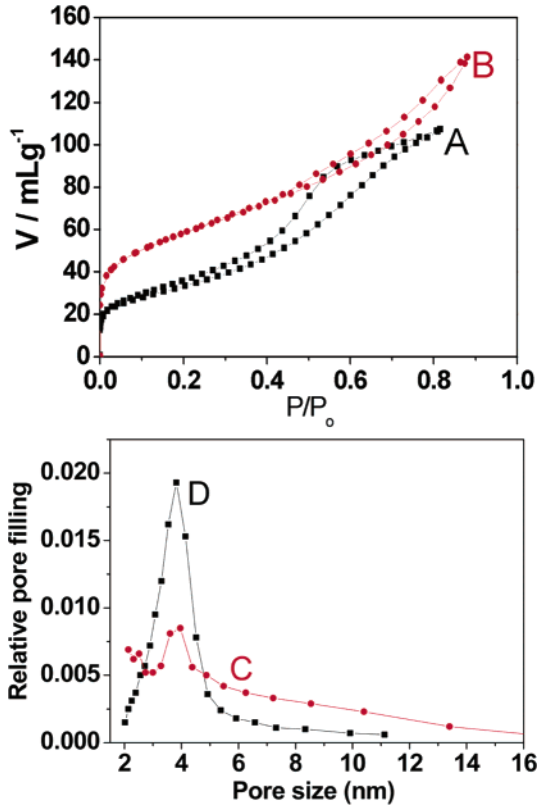

Figure 3. Nitrogen adsorption−desorption isotherms for mesoporous α-Fe_2O_3 (A) with ordered walls and (B) with disordered walls. The lower figure shows the pore size distributions for mesoporous α-Fe_2O_3 (C) with ordered walls and (D) with disordered walls.

139 and 210 $m^2\ g^{-1}$ for the mesoporous α-Fe_2O_3 with ordered and disordered walls, respectively. While we cannot be certain as to the origin of the difference, it is interesting to note that the pore size distribution appears to be somewhat greater in the case of the mesopore with disordered walls; this combined with the high surface area may indicate that the pore surface is rougher for the mesopore with disordered walls.

Structure within the Walls. Turning to the order within the walls, the high resolution image (Figure 1c) demonstrates the high degree of atomic order in the walls of the ordered material. Not only are the walls crystalline but the lattice fringes indicate that there is a considerable degree of structural coherence throughout each particle, implying a near-single crystal-like arrangement of atoms within the walls. This is confirmed by selected area electron diffraction (SAED), Figure 1a inset, which exhibits a single-crystal diffraction pattern. Wide-angle PXRD data for the materials are shown in Figure 4. Well-defined peaks corresponding to the crystal structure of α-Fe_2O_3 are clearly evident, in agreement with the HRTEM and SAED data. Although the high-resolution image of the disordered material, shown in Figure 1f, appears to demonstrate little evidence of order within the walls, a SAED pattern shows several diffraction rings corresponding to the d spacings expected for α-Fe_2O_3 (inset in Figure 1f). This is confirmed by the wide-angle PXRD data in Figure 4, which clearly shows peaks corresponding to α-Fe_2O_3. However, the peaks are weak and broad compared with those for ordered α-Fe_2O_3 (Figure 4B). The SAED and PXRD data indicate that the walls of so-called disordered Fe_2O_3 are not amorphous but contain small crystallites of α-Fe_2O_3 (∼6 nm based on analysis of the PXRD peak widths by the Scherrer

(30) Sakamoto, Y.; Kim, T. W.; Ryoo, R.; Terasaki, O. *Angew. Chem., Int. Ed.* **2004**, *43*, 5231.

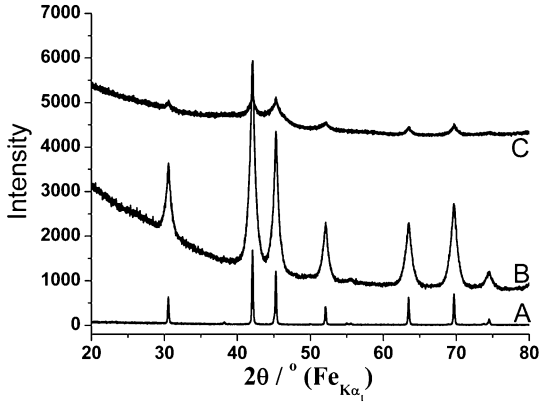

Figure 4. Wide-angle PXRD patterns: (A) bulk α-Fe_2O_3; (B) mesoporous α-Fe_2O_3 with ordered walls; (C) mesoporous α-Fe_2O_3 with disordered walls.

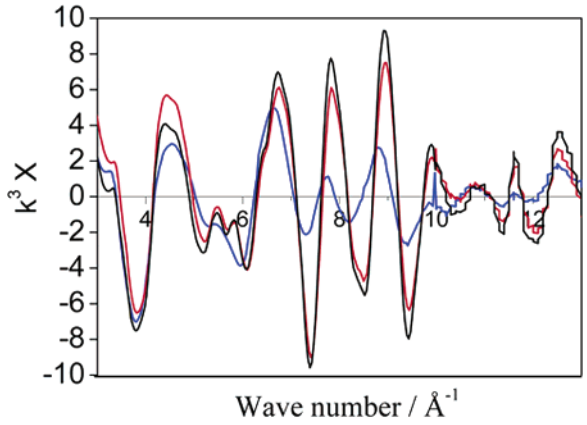

Figure 5. Fe *K*-edge EXAFS spectrum for bulk α-Fe_2O_3 (black line), mesoporous α-Fe_2O_3 with ordered walls (red line), and mesoporous α-Fe_2O_3 with disordered walls (blue line).

formula) that are orientationally disordered with respect to each other. This is consistent with EXAFS analysis presented later. We cannot rule out the coexistence of some amorphous α-Fe_2O_3, but given that iron oxide is not a glass former, it is likely that the walls are composed of the α-Fe_2O_3 nanocrystallites. Note that the wall thickness is ∼7 nm based on the pore dimensions of the KIT-6 template from which the mesoporous Fe_2O_3 is formed. We shall continue to refer to the two forms of mesoporous α-Fe_2O_3 as ordered and disordered, recognizing the fact that the former consist of near-single crystal-like mesoporous particles, whereas the latter possesses α-Fe_2O_3 nanoparticles.

Confirmation that the iron ions are in the +3 oxidation state for both mesoporous materials was obtained by X-ray absorption near-edge structure (XANES) analysis. Extended X-ray absorption fine structure (EXAFS) data collected simultaneously are shown in Figures 5 and 6. Data for bulk α-Fe_2O_3 are shown for comparison. Interatomic distances and *R* factors indicating the goodness-of-fit are shown in Table 1. There is excellent agreement between the Fe−O bond lengths for all three samples, the standard bulk material, and the two mesoporous phases (Figure 6). Considering the next nearest neighbor Fe−Fe distances, it is evident from Figure 6 that there is very good agreement between the crystalline mesoporous α-Fe_2O_3 and the bulk phase, which is not surprising given the extended crystalline nature of the walls in the mesoporous α-Fe_2O_3. Although the Fe−Fe peaks in Figure 6 for the disordered α-Fe_2O_3 mesopore are weaker, three peaks are again apparent corresponding to

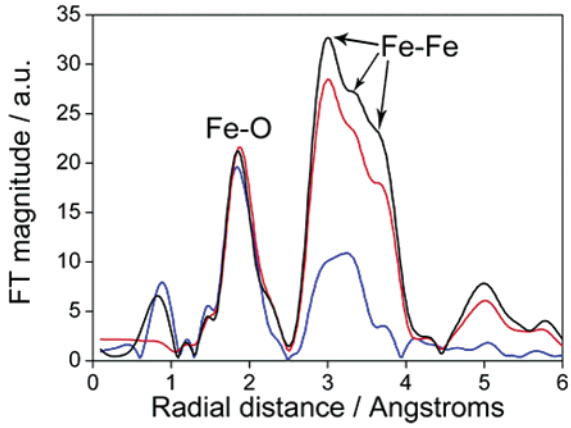

Figure 6. The Fourier transform of the data shown in Figure 5 for bulk α-Fe_2O_3 (black line), mesoporous α-Fe_2O_3 with ordered walls (red line), and mesoporous α-Fe_2O_3 with disordered walls (blue line).

the 3 Fe−Fe distances observed for the crystalline mesopore and the bulk material, consistent with the presence of nanocrystallites of α-Fe_2O_3 in the walls of the disordered material. Reduction in peak intensities as the crystallite size is reduced to the nanometer range has been demonstrated before.[31]

Magnetic Behavior. The magnetic behavior was first investigated by Mössbauer spectroscopy carried out on the two mesoporous α-Fe_2O_3 phases. The results are shown in Figure 7. Data for mesoporous α-Fe_2O_3 with disordered walls correspond to the doublet expected for high-spin Fe^{3+} in an octahedral oxygen environment, where the neighboring spins do not induce order extending over a long range. The quadrupole splitting is 0.76 mm/s, which is consistent with superparamagnetic behavior identified in Mössbauer measurements of nanoparticulate α-Fe_2O_3 with a particle size below 8 nm.[32,33] In other words, the long-range magnetic order present in bulk α-Fe_2O_3 breaks down when the crystalline size is below 8 nm.[32,33] This is consistent with the walls of the disordered material, containing α-Fe_2O_3 nanoparticles of ∼6 nm. The data for mesoporous Fe_2O_3 with ordered walls exhibit the classic sextet spectrum of α-Fe_2O_3 in the bulk phase, typical of the long-range magnetic ordering between spins in this material. The data show that despite the wall thickness in mesoporous α-Fe_2O_3 being less than 8 nm (based on the KIT-6 pore size), Figure 7B, long-range order exists.

We conclude that there are sufficient spin interactions occurring along the walls, that is, within the continuous 2D sheet of α-Fe_2O_3 that forms the walls, to align the neighboring spins. This emphasizes the unique properties of mesoporous α-Fe_2O_3 with ordered crystalline walls.

A more detailed characterization of the unique magnetic properties of mesoporous α-Fe_2O_3 with crystalline walls was carried out by magnetization and neutron diffraction measurements. The results of magnetization measurements are presented in Figure 8. Before considering the magnetism of the mesoporous materials, it is useful to recall the behavior of bulk α-Fe_2O_3. Between the Néel temperature, T_N, of approximately 961 K and the Morin transition temperature, T_M, at ∼265 K, the spins in α-Fe_2O_3 lie flat in the (111) planes of the rhombohedral cell

(31) Davis, S. R.; Chadwick, A. V.; Wright, J. D. *J. Phys. Chem. B* **1997**, *101*, 9901.
(32) Dormann, J. L.; Cui, J. R.; Sella, C. *J Appl. Phys.* **1985**, *57*, 4283.
(33) Zysler, R. D.; Fiorani, D.; Testa, A. M.; Suber, L.; Agnostinelli, E.; Godinho, M. *Phys. Rev. B* **2003**, *68*, 212408.

Table 1. EXAFS Results for Bulk α-Fe_2O_3, Mesoporous α-Fe_2O_3 with Ordered and Disordered Walls

Simplified XRD			Bulk α-Fe_2O_3				Mesoporous α-Fe_2O_3 with ordered walls				Mesoporous α-Fe_2O_3 with disordered walls			
atom	CN	R	atom	CN	R	A	atom	CN	R	A	atom	CN	R	A
O	3	1.957	O	3	1.946	0.017	O	3	1.927	0.013	O	3	1.951	0.019
O	3	2.098	O	3	2.139	0.032	O	3	2.11	0.019	O	3	2.164	0.059
Fe	4	2.97	Fe	4	2.963	0.016	Fe	4	2.954	0.018	Fe	4	3.022	0.034
Fe	3	3.368	Fe	3	3.344	0.022	Fe	3	3.357	0.018	Fe	3	3.383	0.05
O	3	3.392	O	3	3.387	0.005	O	3	3.421	0.006	O	3	3.414	0.027
O	3	3.601	O	3	3.827	0.022	O	3	3.631	0.015	O	3	3.686	0.011
Fe	6	3.704	Fe	6	3.694	0.019	Fe	6	3.692	0.022	Fe	6	3.516	0.106
				$R = 34.38\%$				$R = 33.26\%$				$R = 36.34\%$		

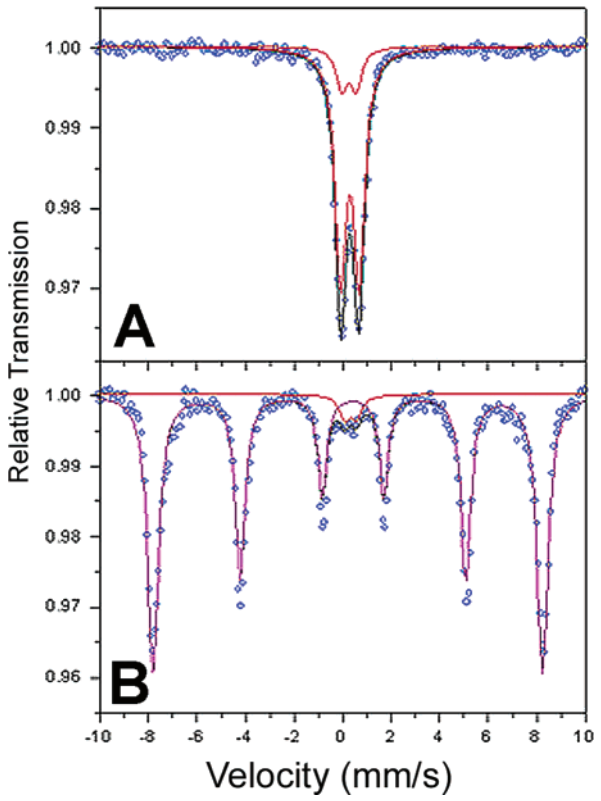

Figure 7. Mössbauer spectra for mesoporous α-Fe_2O_3 (A) with disordered walls and (B) with ordered crystalline walls.

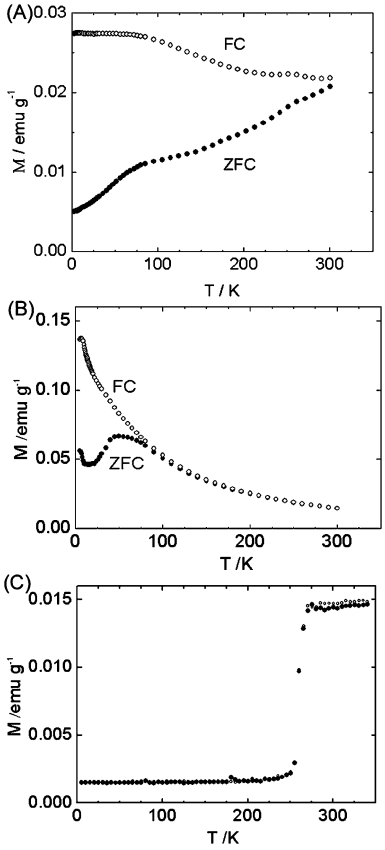

Figure 8. Magnetization data for the mesoporous α-Fe_2O_3 (A) with ordered walls and (B) with disordered walls, taken in 0.01 T after first cooling in zero field (ZFC, closed circles) and then in an applied field of 0.01 T (FC, open circles). (C) Results of the same measurement on bulk α-Fe_2O_3 prepared from the same iron sources with the same heating treatment.

such that the spins in each layer are approximately parallel to each other, but antiparallel to those in adjacent layers.[34−36] A Dzyaloshinski−Moriya interaction[37,38] gives rise to a small canting of moments within each (111) plane, and these produce a new ferromagnetic moment of the order of 0.005 μ_B/iron atom. This phase is referred to as the weakly ferromagnetic (WF) form. Below T_M, the moments rotate through almost 90° to lie nearly parallel or antiparallel to the [111] direction.[39−42] This phase—referred to as the antiferromagnetic (AF) form—has no net magnetization, and so a sharp drop in susceptibility is expected at T_M. The sample of bulk α-Fe_2O_3 shows this very clearly (Figure 8C).

The ordered mesoporous material shows a splitting between the field-cooled (FC) and zero-field-cooled (ZFC) data from the highest experimental temperature, compatible with some degree of spontaneous moment over the entire temperature range studied. There are also features suggestive of magnetic transitions in the region of 260 and 75 K. The first of these is close to the Morin transition temperature, T_M, of bulk α-Fe_2O_3. However, the expected sharp drop in susceptibility at the Morin temperature does not occur, suggesting that mesoporous α-Fe_2O_3 with ordered walls does not go through such a transition over the temperature range of our measurements. It is well-known that the Morin transition is sensitive to the size of the structural domains in α-Fe_2O_3—so, for example, T_M is less than 4 K for α-Fe_2O_3 particles of diameter 8−20 nm.[32,33,43−47] It is possible

(34) Morin, F. J. *Phys. Rev.* **1950**, *78*, 819.
(35) Neel, L.; Pauthenet, R. *Compt. Rend.* **1952**, *234*, 2172.
(36) Shull, C. G.; Strauser, W. A.; Wollan, E. O. *Phys. Rev.* **1951**, *83*, 333.
(37) Dzyaloshinski, I. *JETP* **1958**, *6*, 1120.
(38) Moriya, T. *Phys. Rev.* **1960**, *120*, 910.
(39) Nathans, R.; Pickart, S. J.; Alperin, H. A.; Brown, P. J. *Phys. Rev.* **1964**, *136*, A1641.
(40) Foner, S.; Williamson, S. J. *J. Appl. Phys.* **1965**, *36*, 1154.
(41) Besser, P. J.; Morrish, A. H.; Searle, C. W. *Phys. Rev.* **1967**, *153*, 632.
(42) Morrish, A. *Canted antiferromagnetism: hematite*; World Scientific: River Edge, NJ, 1994.
(43) Kundig, W.; Bommel, H.; Constabaris, G.; Lindquist, R. H. *Phys. Rev.* **1966**, *142*, 327.

that the confined dimension of the walls plays a role in suppressing T_M. In summary, despite the fact that understanding the transition at 265 K in the ordered material will require further study, we can draw the important conclusion that the confined dimensions of crystalline α-Fe_2O_3 in the ordered mesoporous material are sufficient to suppress the Morin transition but not to suppress the long-range magnetic order.

The feature in the magnetization in the region of 75 K is also difficult to assign. Transitions of a similar form are observed in ferrihydrite, $Fe_2O_3 \cdot nH_2O$, but we believe it is very unlikely that any of this material is formed during the synthesis.[48−51] It is more likely that this feature arises from a few regions of the sample composed of small crystallites and behaving more like finely particulate α-Fe_2O_3 than the bulk material.[32,33,43−47] Such particles may possess a spontaneous magnetization down to 5 K that is as large as that observed in the WF phase of the bulk material and behave as superparamagnets at room temperature. On cooling, a blocking transition has been observed at a temperature, T_B, which is expected to depend on particle size: for example, for particles of 16 nm diameter, T_B is in the region of 25−30 K.[45] It is conceivable therefore that the transition we observe around 75 K stems from regions of the material with short structural coherence lengths.

The most prominent feature of the susceptibility data for the mesoporous α-Fe_2O_3 with disordered walls is a cusp near 50 K, above which there is FC-ZFC divergence. There is no sign of a Morin transition near that of the bulk material. In both respects, the collective magnetic properties of this material have similarities with those of small particles of α-Fe_2O_3, with the suppression of the Morin transition and some form of blocking transition at a temperature that depends on the nature of the structural correlation length.

To examine the magnetic order in mesoporous α-Fe_2O_3 with crystalline walls in more detail, neutron powder diffraction data were collected at room temperature. These data are shown in Figure 9, together with the Rietveld fit, performed using the GSAS package. The diffraction peaks are significantly broadened with respect to the instrument resolution of the neutron diffractometer. In addition to the diffraction peaks from the hematite crystal structure, peaks characteristic of the long-range magnetic order of the Fe^{3+} moments are observed. Most prominent is the peak centered near 4.6 Å, which may be indexed as [003] in the hexagonal setting of space group $R\bar{3}c$. This is characteristic of the WF magnetic phase and absent in the AF phase. Rietveld refinement of the data was performed in space group $R\bar{3}c$, with Fe at (0, 0, *z*) and O at (*x*, 0, 1/4). The magnetic structure was refined in the space group *P*1, with the same dimensions as the nuclear unit cell and, initially, the same disposition of moments found in the AF phase of bulk α-Fe_2O_3. The form factor for Fe^{3+} was the spherical $\langle j_0 \rangle$ expansion

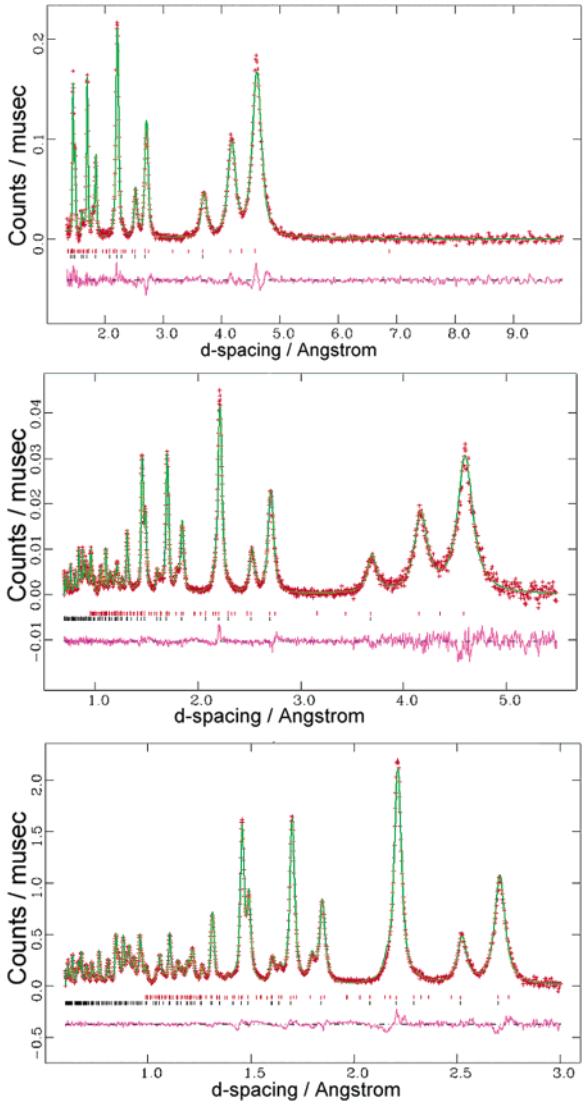

Figure 9. Powder neutron diffraction pattern for α-Fe_2O_3 with ordered walls collected at 298 K on three different detector banks at ROTAX: from top to bottom, the angle of the banks are at $2\theta = 21.9$, 61.5, and 120.9°, respectively. In each case, the data (crosses) have been fitted (upper line through the data points) by Rietveld analysis to a nuclear and magnetic structure, depicted by the lower and upper tick marks, respectively. The line at the bottom of each plot represents the difference between the data and the calculated profile.

implemented in GSAS. The introduction to the refinement of a component of a moment perpendicular to the hexagonal *c*-axis led to an unstable refinement and did not improve the fit, so it was abandoned; the small ferromagnetic component perpendicular to the hexagonal *c*-axis was neglected in these calculations. Refined parameters are in good agreement with previous studies of the crystal and magnetic structure and are as follows: $a = b = 5.03726(1)$ Å; $c = 13.7663(5)$ Å; cell volume = 302.497(13) Å^3; z(Fe) = 0.354986(35); u(Fe) = 0.0097(2) Å^2; x(O) = 0.3074(1); u(O) = 0.0075(2) Å^2; magnetic moment of $Fe^{3+} = 4.02(2)\ \mu_B$ parallel to the hexagonal *c*-axis; weighted R(wp) 2.3%; $\chi^2 = 1.9$.[36,39,52,53] The results of the neutron diffraction confirmed the existence of long-range magnetic order in the mesoporous α-Fe_2O_3 with crystalline walls.

(44) Amin, N.; Arajs, S. *Phys. Rev. B* **1987**, *35*, 4810.
(45) Bodker, F.; Hansen, M. F.; Koch, C. B.; Lefmann, K.; Morup, S. *Phys. Rev. B* **2000**, *61*, 6826.
(46) de Boer, C. B.; Mullender, T. A. T.; Dekkers, M. J. *Geophys. J. Int.* **2001**, *146*, 201.
(47) Gee, S.-H.; Hong, Y.-K.; Sur, J. C.; Erickson, D. W.; Park, M. H.; Jeffers, F. *IEEE Trans Magn.* **2004**, *40*, 2691.
(48) Cornell, R. M.; Schwertmann, U. *The iron oxides*; VCH: Weinheim, Germany, 1996.
(49) Seehra, M. S.; Punnoose, A. *Phys. Rev. B* **2001**, *64*, 132410.
(50) Zergenyi, R. S.; Hirt, A. M.; Zimmermann, S.; Dobson, J. P.; Lowrie, W. *J. Geophys. Res.* **2000**, *105*, 8297.
(51) Seehra, M. S.; Babu, V. S.; Manivannan, A.; Lynn, J. W. *Phys. Rev. B* **2000**, *61*, 3513.
(52) Blake, R. L.; Hessevick, R. E.; Zoltai, T.; Finger, L. W. *Am. Mineral.* **1966**, *51*, 123.
(53) Shirane, G.; Cox, D. E.; Takei, W. J.; Ruby, S. L. *J. Phys. Soc. Jpn.* **1962**, *17*, 1598.

Conclusions

α-Fe_2O_3 with an ordered mesoporous structure and crystalline walls has been prepared for the first time and compared with α-Fe_2O_3 with an ordered mesoporous structure and disordered walls. The former exhibits near-single crystal-like order throughout the walls of each particle, whereas the walls of the latter contain nanocrystallites of α-Fe_2O_3 ($\sim$6 nm) that are orientationally disordered with respect to each other. The magnetic behavior of mesoporous α-Fe_2O_3 with disordered walls is consistent with that of α-Fe_2O_3 nanoparticles of less than 8 nm, that is, no long-range magnetic order, absence of a Morin transition, and the presence of superparamagnetic behavior. The magnetic behavior of mesoporous α-Fe_2O_3 with crystalline walls is unique. Mössbauer, magnetization susceptibility, and powder neutron diffraction all indicate that, despite the wall thickness being less than 8 nm, long-range magnetic ordering persists due to interaction between Fe^{3+} ions along the walls. The material exhibits weakly ferromagnetic susceptibility and Bragg scattering characteristic of the WF phase of bulk α-Fe_2O_3. However, the confined dimensions are sufficient to suppress the Morin transition present in bulk α-Fe_2O_3.

Acknowledgment. P.G.B. is indebted to the Royal Society, EPSRC, and the EU for financial support.

Supporting Information Available: Full citation of ref 17. This material is available free of charge via the Internet at http://pubs.acs.org.

JA0584774